JOURNAL OF MATERIALS SCIENCE **37** (2002) 2927–2935

Microstructural evolution in nanocrystalline alumina containing silicate glasses

S. K. SAHA, R. CHAIM
Department of Materials Engineering, Technion—Israel Institute of Technology, Haifa 32000, Israel
E-mail: rchaim@tx.technion.ac.il

Pure nanocrystalline δ-alumina powders were coated with different fractions (5, 10, and 15 vol%) of SiO_2-SrO glass using the sol-gel technique. The isostatically cold pressed powders were pressureless sintered in air for 5 h in the temperature range of 1250°C to 1550°C. The relative densities were ranged between 60 to 90% of the theoretical and were composition dependent. The density was increased with the sintering temperature. In pure alumina, the δ to α phase transformation went to completion by sintering at 1250°C. However, in the glass-coated samples, transition δ-alumina was mostly retained after sintering at the same temperature. Pure nanocrystalline alumina sintered at 1350°C exhibited vermicular structure with isolated pores. The microstructure of the low glass-containing samples exhibited nanocrystalline to submicron size grains arranged in platelet-shaped clusters. Samples with higher glass contents exhibited also micron-size needle-shape grains of strontium aluminate.

1. Introduction

Alumina is a very common engineering oxide ceramic used in different structural applications. It is characterized by several polymorphs [1]. From morphological point of view, the transition aluminas powders often form with very fine particle size in the nanometer range. Sintering and densification of the nanocrystalline transition aluminas generally lead to the formation of the high temperature stable form, corundum (α-alumina), and accompanied by explosive grain growth [2]. Thus, the fabrication of dense nanocrystalline oxide ceramics in general, and of alumina in particular, is very challenging.

Recent studies on sintering and densification of nanocrystalline ceramics have highlighted the problem of achieving high densities (>90% of the theoretical density) without excessive grain growth [3–8]. It has been shown by Averback *et al.* [4] and Mayo and Hague [5] that grain growth in nanocrystalline oxides is enhanced during sintering when the density approaches >90% of the theoretical density. Consequently, sintering processes that require lower temperatures or shorter durations were adopted. Recently, microwave-sintering [7], plasma assisted sintering [8], as well as high pressure sintering [9, 10] of nanocrystalline transition alumina were reported. Two important observations were made [8]: (a) transition aluminas require much higher homologous temperatures for achieving equivalent densities compared to other nanocrystalline ceramics and (b) best densities obtained were <90% of the theoretical, while retaining the grain size below 100 nm.

The difficulties in obtaining high density nanocrystalline samples is also due to the fact that the sintering temperatures during pressureless and low-pressure sintering are higher than the phase transformation temperature (~1200°C) to α-alumina. Mishra *et al.* [8] suggested that higher sintering pressures or the use of additives can assist achieving higher densities with the nanocrystalline structure. During reactive hot pressing of aluminum hydroxides, large necks were formed between the particles that resulted in a strong network. Thus higher pressures to break up the network, or higher temperatures to promote diffusional processes, were required to achieve high density α-alumina [11, 12].

Hot-pressing of the nanocrystalline γ-alumina in the temperature range of 650°C to 1100°C under high pressures led to the reduction of the γ to α transformation temperature from 1200°C at 1 atm to about 750°C at 1 GPa. Fully dense samples with a grain size of ~142 nm were obtained at 1000°C to 1100°C, and 1 GPa within 10 minutes [13]. Nordahl and Messing [14] studied the transformation and densification of nanocrystalline θ-alumina during sinter-forging. Using seeded nanocrystalline θ-alumina as starting material, dense α-alumina with an average grain size of 230 nm was formed at 280 MPa/1060°C for 30 minutes.

On the other hand, the high pressure techniques are limited to fabrication of small samples which are not appropriate for mechanical tests. However, glass additions may be used to increase the phase transition temperature [5] and enable, in turn, to preserve the nanocrystalline character at lower sintering temperatures [15]. This approach is appropriate especially

where the glassy phase intended to enhance the superplastic behavior of the nanocrystalline ceramic.

In the present study, nanocrystalline δ-alumina powder was coated with variable amounts of the glassy phase. The effect of the glass coating on the sintering behavior and the microstructural evolution of the nanocrystalline alumina was studied.

2. Experimental

Commercial spherical nanocrystalline alumina powder (Neomat) was used as the precursor powder. The mean particle size was determined by transmission electron microscopy (TEM) to be 50 nm. The crystalline phase was determined as δ-alumina using X-ray diffraction (XRD). The alumina powders were coated with glass by the sol-gel technique. The binary glass composition of SiO_2-SrO (60 : 40 mole ratio) was chosen according to the glass forming region in the Al_2O_3-SiO_2-SrO ternary phase diagram [16]. Different stages of the sol-gel glass coating technique were shown in Fig. 1. An ethanol-water solution corresponding to the initial composition of the glass was prepared by dissolving tetraethoxysilane in ethanol and strontium nitrate in water. Appropriate amount of the glass solution (according to the 5, 10 and 15 vol% glass content with respect to alumina) was added to the aqueous slurry of alumina with ultrasonication for proper mixing. The resultant slurry was stirred (magnetic stirrer) while slowly heating it to dryness. The resultant powders were gently ground in agate mortar and annealed for 2 h in air at 400°C. The glass-coated powders were analyzed by XRD (Cu-K_α radiation, 40 kV, 30 mA) for phase analysis. The thickness and homogeneity of the glass coating, when possible, were characterized using TEM.

The pure and glass-coated powders were uniaxially pressed into disc-shaped pellets of 15 mm diameter and 2 to 4 mm thickness, followed by cold isostatic pressing (CIP) at 250 MPa. The green density of the pellets was measured by weighing. Selected green compacts were used in dilatometer to determine the phase transition temperature and the shrinkage characteristics. Sintering experiments were performed in air for 5 h at the temperature range of 1250°C to 1550°C using a heating rate of 5°C/min. The final densities of the samples were determined by the Archimedes method. Sintered specimen surfaces as well as polished and thermally etched surfaces were characterized using high resolution scanning electron microscopy (HRSEM).

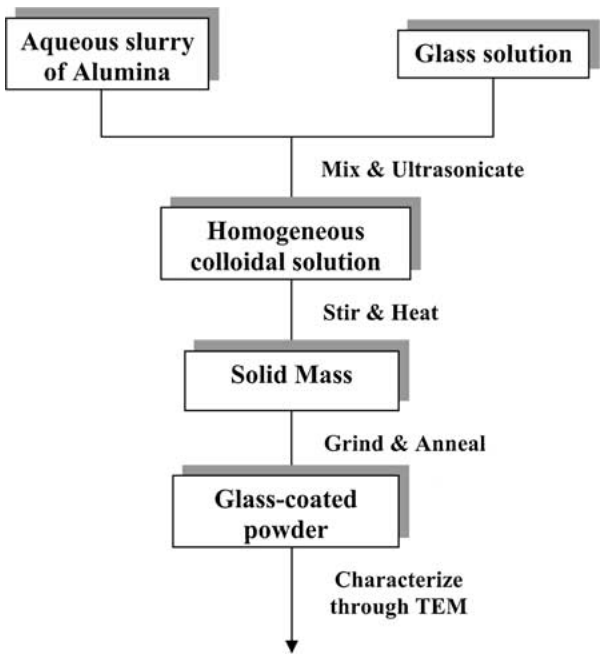

Figure 1 Schematic diagram of the glass coating experiment.

3. Results and discussion

3.1. Powder morphology

The nanocrystalline alumina powder was composed of agglomerate-free spherical single grains (Fig. 2a) with the mean particle diameter (d_{50}) of 50 nm. The particle size distribution was determined to be log-normal using

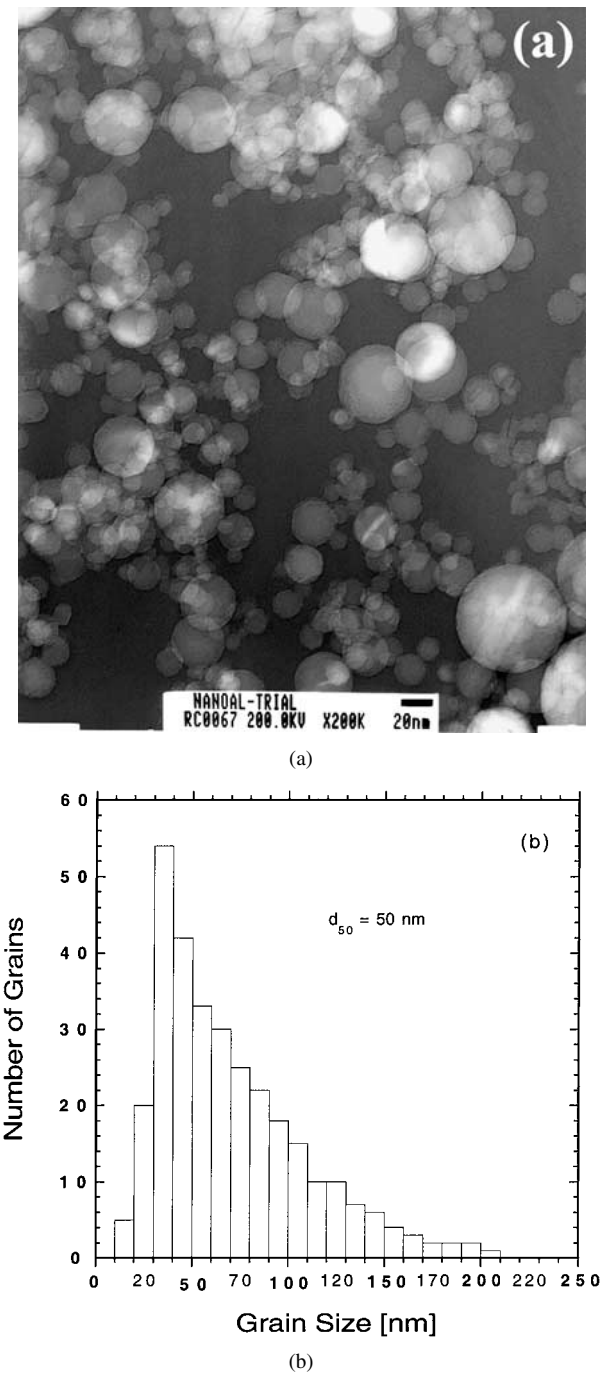

Figure 2 (a) Transmission electron micrograph of pure δ-alumina, and (b) particle size distribution exhibiting the log-normal characteristic.

Figure 3 Transmission electron micrograph of the 15% glass-coated δ-alumina.

TEM images (Fig. 2b). The powder morphology and the distribution of the glass coating on the alumina particle are shown in Fig. 3. The glass coating was well resolved in the powders coated with 15 vol% glass. The coating was featureless, in contrast to the crystalline alumina particles. The coating thickness varied between 1 to 4 nm from particle to particle. Nevertheless, the coating was homogeneously applied to the particle surfaces, following the circular contour of the grains (in the cross section view) (Fig. 3). However, the coating thickness was not resolved clearly in the powders coated either with 5% or 10% glass. Due to high surface area of the initial alumina powder, relatively large amount of the glass is required to make the glass coating thick enough for microscopic observations.

3.2. Phase analysis

X-ray diffraction (XRD) spectrum of the pure alumina powder was consistent with transition δ-alumina (Fig. 4). Glass-coated powders after drying and annealing for 2 h at 400°C showed additional peaks from strontium nitrate (Fig. 4) indicating that some residual nitrate was left. Pure δ-alumina was fully transformed to α-alumina after sintering at 1250°C for 5 h (Fig. 5). Nevertheless, after sintering at the same conditions, the glass-containing samples retained their transition δ-alumina phase. Therefore, the glass coating has a remarkable effect on the phase transition temperature. XRD patterns of the pure and the glass-containing aluminas sintered at 1350°C or above it exhibited full transformation of δ-alumina to α-alumina (Fig. 6). Sintered glass-containing samples contained additional intermediate phase along with formation of α-alumina. Significant amount of strontium aluminate ($SrAl_{12}O_{19}$) was formed in the form of needle-shape crystals (see below) on the sintered surfaces of the 15 vol% glass-coated pellet. This phase was also noticed, albeit in smaller proportion, in the 5% and 10% glass-coated samples. Formation of this secondary crystalline phase indicates that the glass content may further be decreased.

It is worth to note that no detectable mullite peaks were observed in the XRD spectra. This may arise due to the difficulties in nucleation of mullite at the interface in the silica-coated alumina powders [17]. Such nucleation occured at higher temperatures ($\geq$1500°C) than needed for nucleation in the sol-gel derived aluminosilicate [18] and is composition dependent [19, 20].

3.3. Densification and sintering

The linear shrinkage of the pure and the glass-coated alumina samples versus temperature are shown in

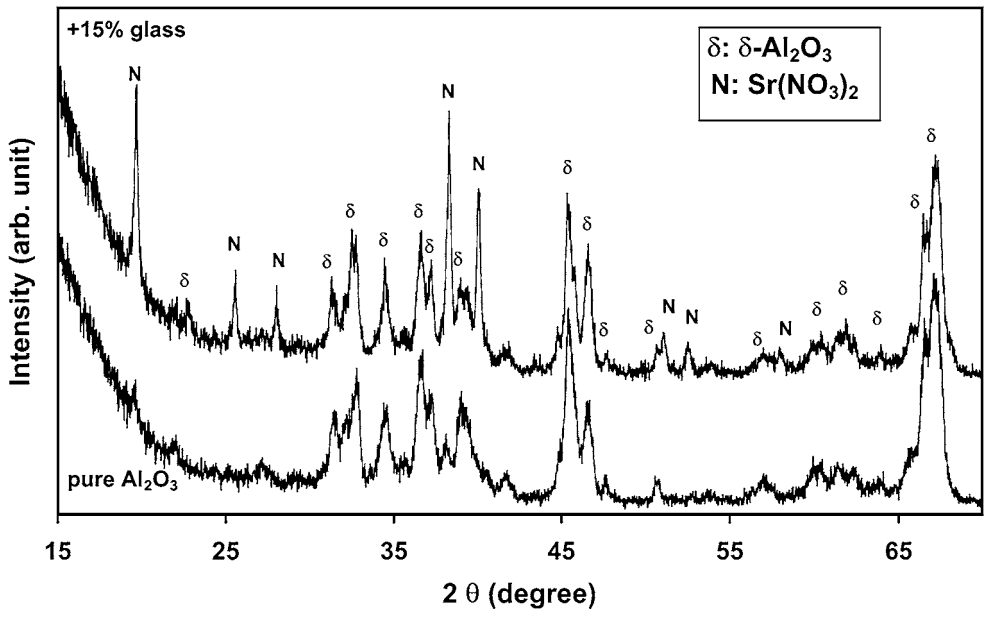

Figure 4 XRD patterns of pure neomat alumina and 15% glass-coated powder annealed at 400°C for 2 h.

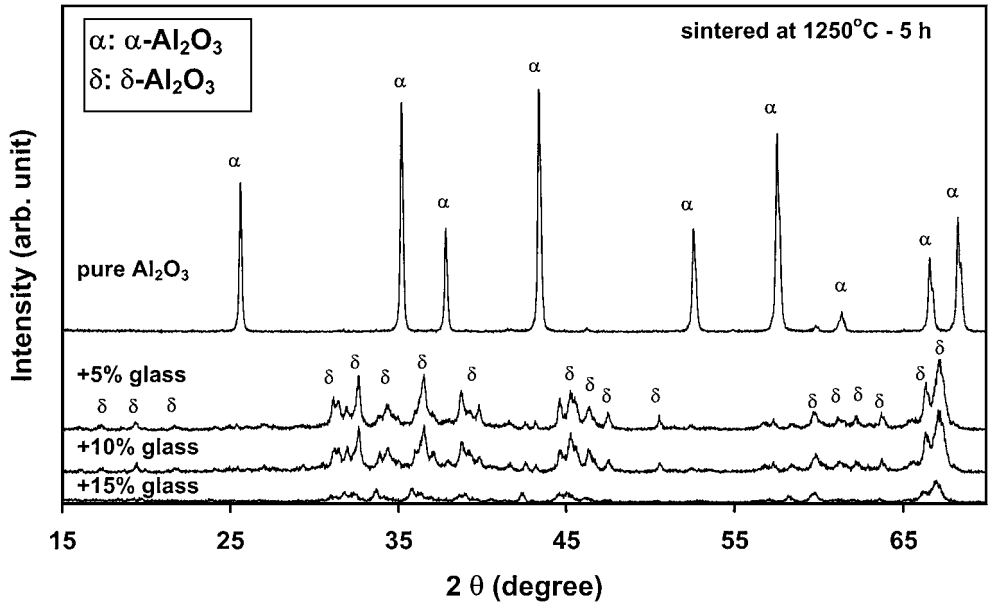

Figure 5 XRD patterns of pure and glass-coated powder compacts sintered at 1250°C for 5 h.

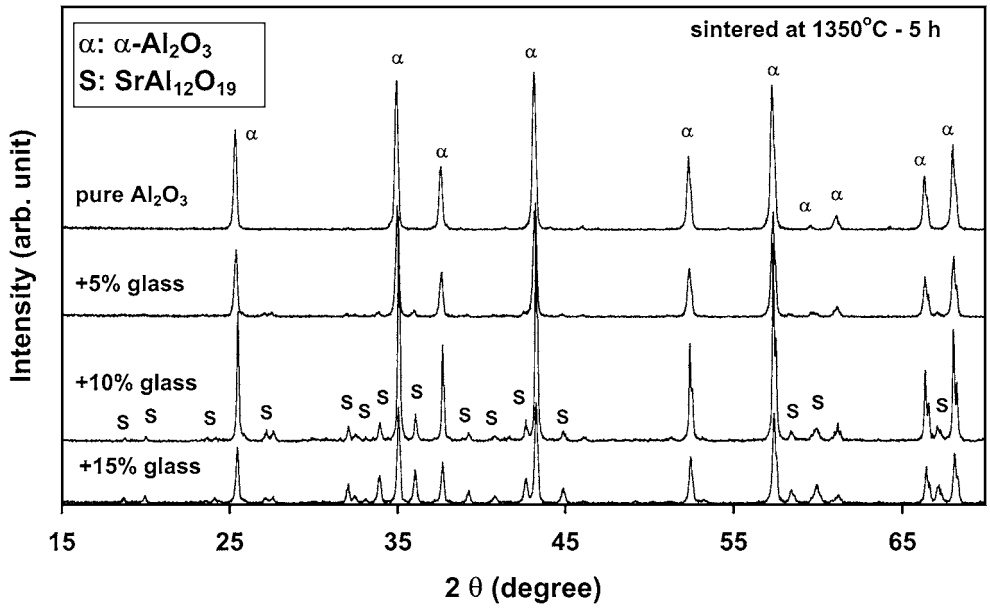

Figure 6 XRD patterns of pure and glass-coated powder compacts sintered at 1350°C for 5 h.

Fig. 7. Densification and shrinkage of the glass-coated alumina starts at a relatively lower temperature (1000°C for 15 vol% glass) with respect to pure alumina sample (1100°C). This may points to enhanced particle rearrangement and densification, due to the presence of the glassy coating. The presence of glass also increases the δ to α-alumina phase transformation temperature. In the pure alumina samples, this transformation occurred at 1200°C, as was evinced from the rapid decrease in the densification rate. The phase transformation temperature was increased to 1400°C for the 15 vol% glass-coated sample. The absolute shrinkage as well as the densification rate were higher in the later pellets prior to the transformation temperature.

Densification pattern of the pure and the glass-coated nanocrystalline alumina compacts with respect to the sintering temperature (for 5 h duration) were summarized in Fig. 8. The green density of the cold isostatically pressed compacts was about 55% of the theoretical density, irrespective of the sample composition. At 1250°C for 5 h, the samples start sintering with negligible densification. At this temperature, the lower glass-containing compacts exhibited lower densities, albeit the density increased with the glass content. This effect should be related to lack of densification that is associated with the phase transformation to stable alumina in these compacts. Nevertheless, increase in the glass content is expected to enhance the particle rearrangement as well as the interfacial diffusion processes that promote densification. This phenomenon is supported by the dilatometric results. At 1250°C, pure alumina is expected to be in the α-corundum structure. Therefore, the sample has been benefited from the ~9% volume shrinkage which is accompanied to the δ- to α-phase transformation in alumina [21]. Increase in the sintering temperature to 1350°C, 1450°C, and 1550°C for 5 h,

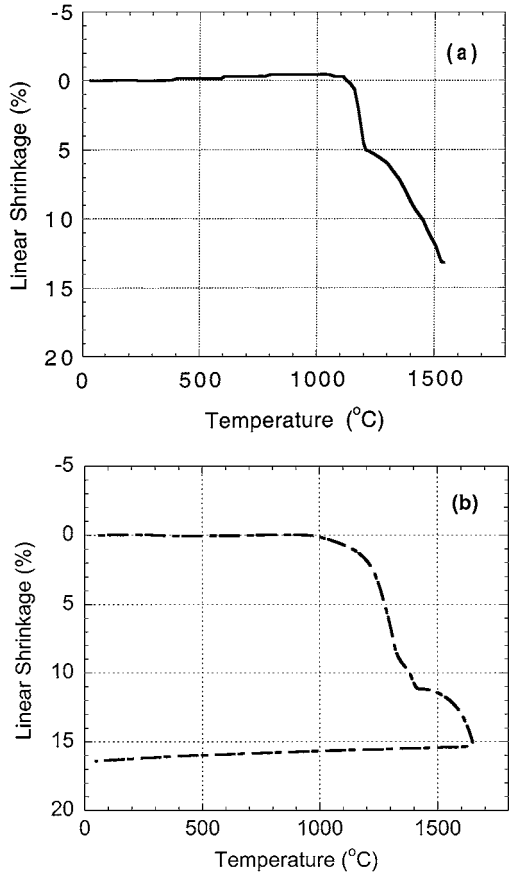

Figure 7 Dilatometric shrinkage curves versus temperature for (a) pure nanocrystalline δ-alumina, and (b) 15% glass coated δ-alumina.

caused the systematic increase in the final density of the pure alumina (70%, 78%, and 84% respectively). Nevertheless, significant increase in the final densities was observed in the glass-containing samples at 1350°C, compared to pure alumina. This differential increase in density may be related to the phase transformation that is expected to occur above 1250°C, in addition to the conventional densification shrinkage. Further increase of the sintering temperature to 1450°C and 1550°C was accompanied by the moderate increase in density.

The absolute density value in each sample, in its dense version, depended upon composition and heat treatment. The glass-coated samples resulted in different phase assemblage; it was consisted of either transition or stable alumina together with either glassy or intermediate crystalline phases (i.e., strontium aluminate). However, since the density of $SrAl_{12}O_{19}$ is 3.985 $g \cdot cm^{-3}$ very close to that of α-alumina (3.987 $g \cdot cm^{-3}$), the density results should be treated with some confidence. In this respect, the maximum error in the calculated density was estimated to be ~1%.

3.4. Sintered microstructure

Effects of the glass coating and the phase transformation on the as-sintered surface microstructure were illustrated in Fig. 9. In order to check the effect of the glass segregation to the pellet surfaces, as-sintered surfaces were characterized both prior to and after the ceramographic preparation. Pure nanocrystalline alumina after sintering at 1350°C for 5 h exhibited vermicular structure with network of pores (Fig. 9a). The original ultrafine grains were found to form micron-size clusters (2 to 5 μm in diameter). Such microstructure is characteristic for the partially sintered pellet that accompanied by the δ- to α-alumina phase transformation. Nevertheless, it still may consist some transition alumina grains. This phase transformation occurs along with decrease in the specific volume, which favors the retainment of the pore networks during sintering. In this respect, glass addition was found to strongly affect this sintered microstructure. The 5 vol% glass-coated sample exhibited much finer microstructure (i.e., sub-micron grain size) on the as sintered surfaces (Fig. 9b). The original alumina grains were found to preserve their spherical shape. Nevertheless, these ultrafine grains were aranged in a few micron-size platelet-shaped clusters (i.e., Fig. 10a). On the other hand, the microstructure of the 10 vol% glass-coated sample contained the ultrafine grains together with micron-size needle-shaped crystals (Fig. 9c). These needle-shaped grains covered the low area fraction of the sample surface, (less than 20%) and represent the $SrAl_{12}O_{19}$ phase. Further increase in the glass content to 15 vol% has led to sintered surface microstructure that mainly was composed of the needle-shaped crystals (Fig. 9d). The observed

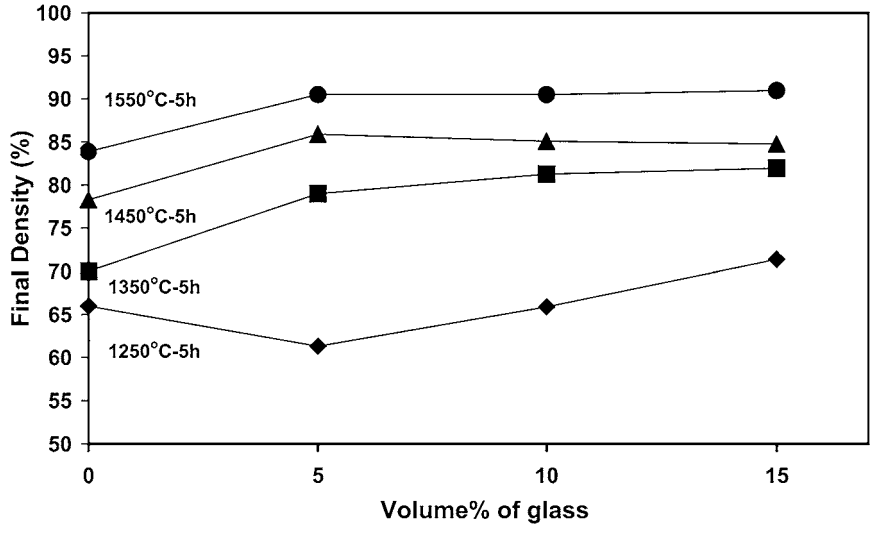

Figure 8 Final density of the pure and glass-coated alumina versus the glass content at different sintering temperatures.

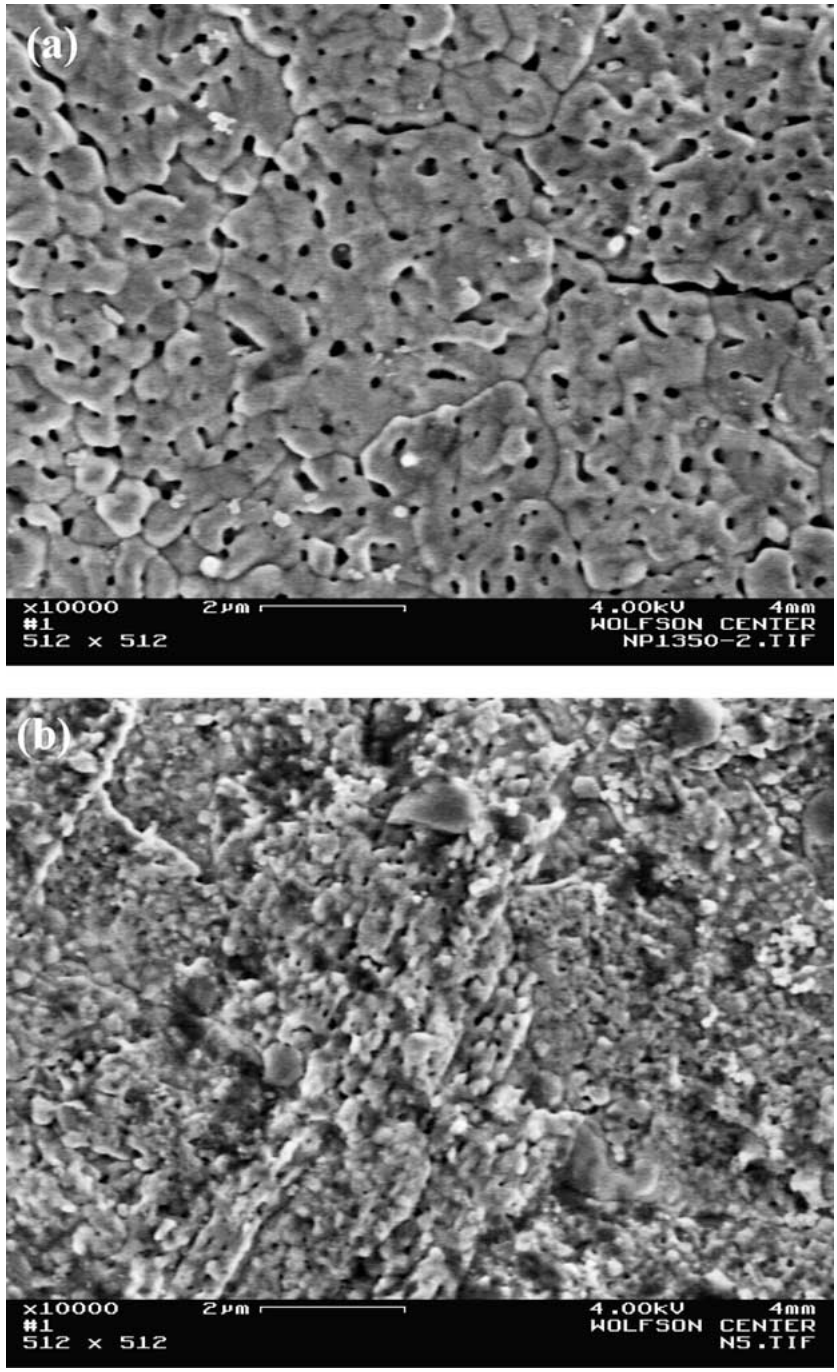

Figure 9 HRSEM images of the pure and glass-coated samples sintered at 1350°C for 5 h. (a) pure alumina, (b) alumina + 5% glass, (c) alumina + 10% glass, (d) alumina + 15% glass. (*Continued.*)

area fraction of these needles on the as-sintered surfaces was far above that expected from the equilibrium phase assemblage of the alumina/strontium aluminate, and indicated on segregation of the glass to the pellets surfaces. The presence of strontium aluminate was confirmed by XRD analysis of the as-sintered glass-coated samples.

The microstructure of the sintered pellets (1350°C for 5 h), after polishing and thermal etching, is shown in Fig. 10. Polishing of the sample surfaces revealed the bulk microstructure where the relative amount of the needle-shaped intermediate phase was significantly reduced. The microstructure of the sample with 5 vol% glass did not change significantly, revealing the ultrafine sub-micron size grains arranged within the platelet-shaped clusters (Fig. 10a). However, in the sample with 15 vol% glass, the intermediate needle-shaped phase was still present but only in a few grain boundary pockets (Fig. 10b). It was apparent that the platelet shaped clusters in the glass-coated samples were composed of the ultrafine alumina grains. These clusters resemble the begining of the anisotropic growth of the alumina grains, most possibly due to the presence of the silicate/rare-alkaline oxide additives [22].

Segregation of the rare-alkaline cations, i.e., Mg and Ca from the intergranular silicate films to the grain boundary surfaces are well documented [23]. Strong segregation of Ca at the Al_2O_3 grain boundaries were reported [24, 25]. The nominal composition of the amorphous grain boundary phase was determined as

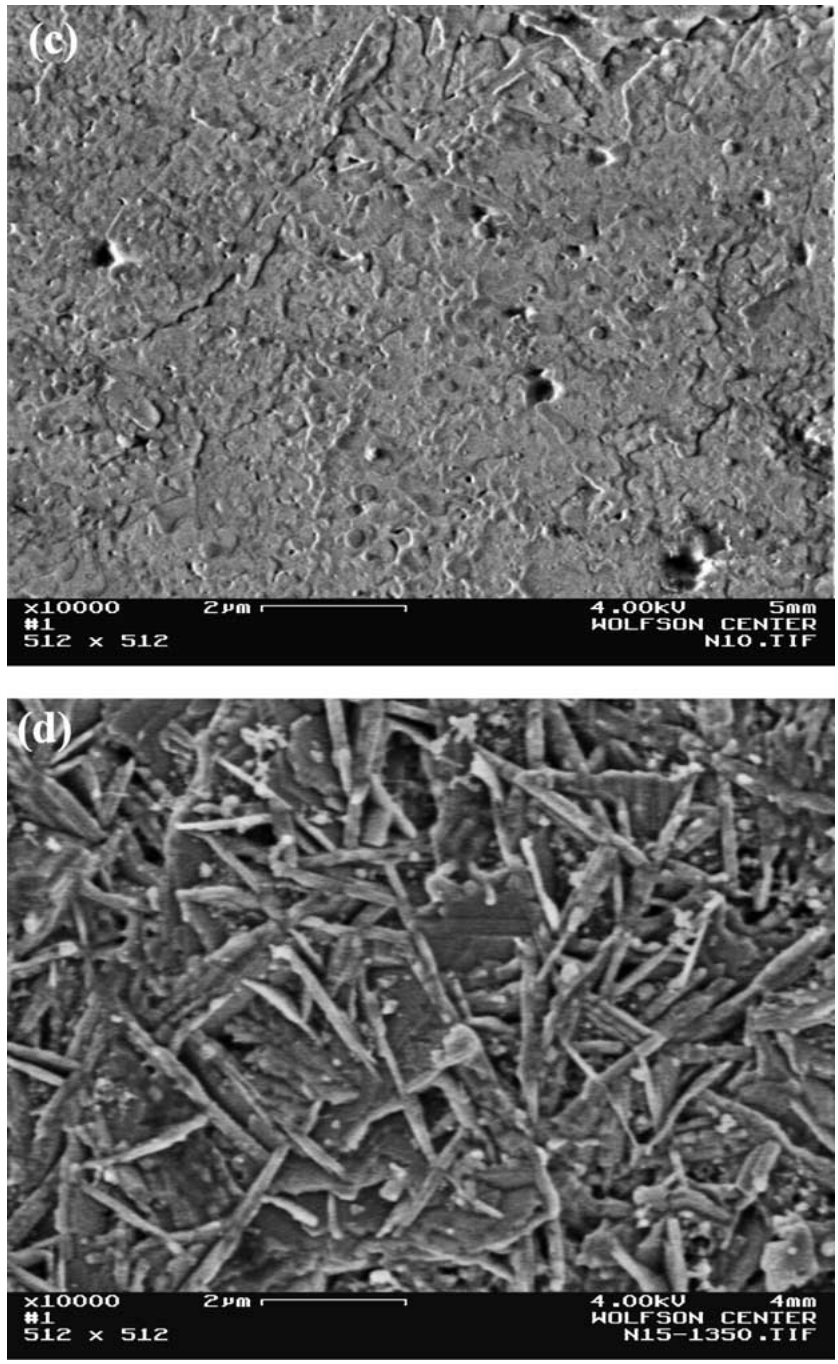

Figure 9 (*Continued.*)

$CaO \cdot 6Al_2O_3$, very close to the intermediate calcium-hexa-aluminate phase. Similarly, addition of 5 wt% SrO to nanocrystalline alumina was found both to enhance the densification and inhibit the grain growth in nanocrystalline alumina compacts [26]. Silica has very limited solubility in alumina. Moreover, crystallization of mullite may occur only at higher temperatures, as was discussed above. This may explain preferable formation of the $SrAl_{12}O_{19}$ phase instead of mullite; the residual silica may be left amorphous at the grain junctions.

The present findings lead to several important observations. As was observed in the zirconia systems [27], SrO acts as surface-active agent that enhances segregation of the grain boundary glassy phase to the external surfaces during sintering and grain growth. As a result, the excess glass tends to segregate from the glassy pockets at the grain boundary junctions (triple lines and quadruple nodes) to the specimen surface, leaving a very thin glassy layer (a few nanometer thick) at the grain boundaries. The grain boundary glassy phase is expected to have an equilibrium thickness [24, 28] and thus is hard to crystallize due to its confined nature by the grains. The excess glass left at the glassy pockets could be crystallized. Such microstructural evolution is expected to improve the conditions for grain boundary sliding at elevated temperatures, provided minimum glass pockets. The presence of bulky glassy phase pockets is expected to promote cavitation depending on the glass properties. Thus, careful optimization of the glassy phase content (below 5 vol%) is needed to form sintered nanocrystalline alumina with appropriate microstructure for the superplastic deformation.

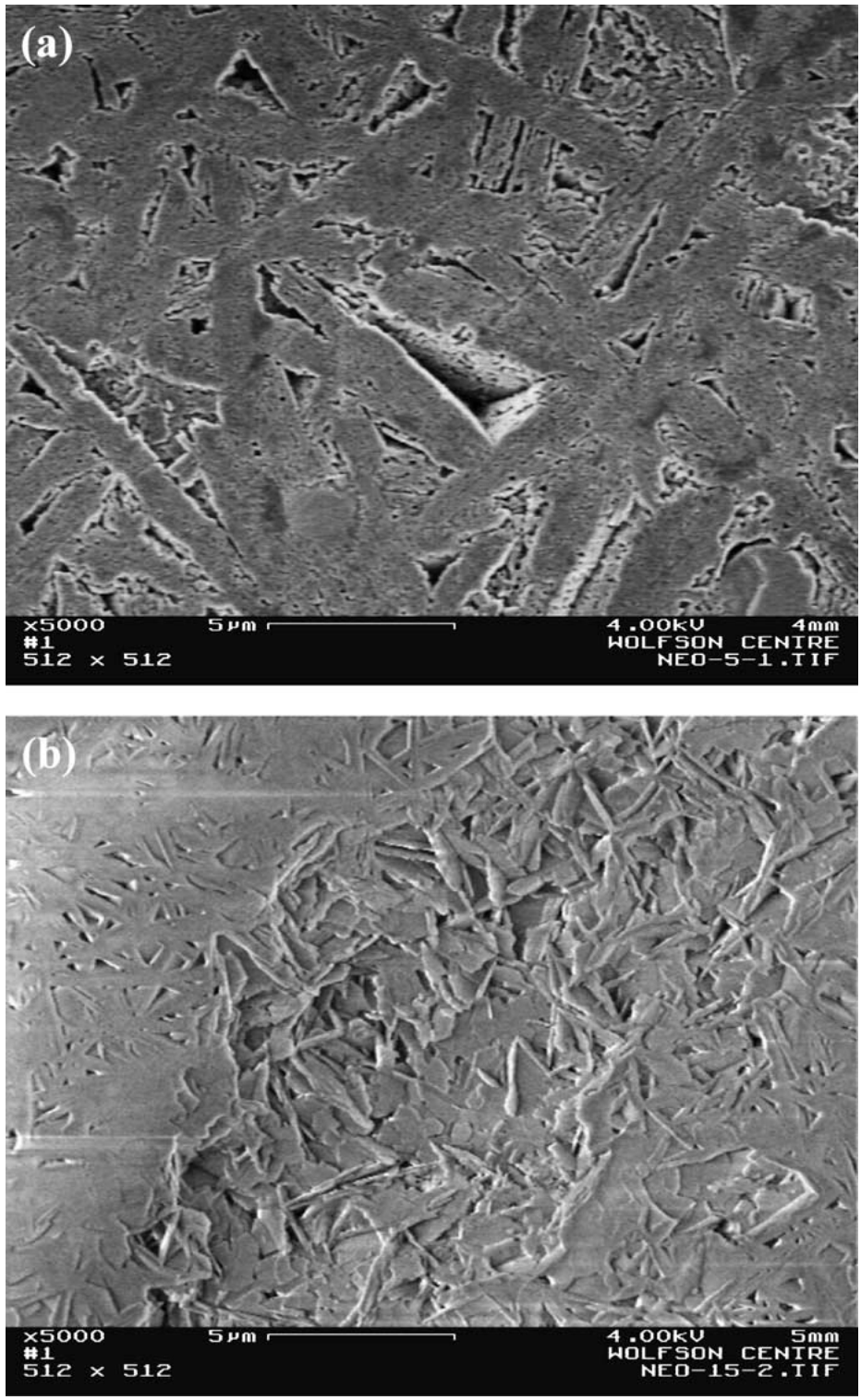

Figure 10 HRSEM images of the polished and thermally etched surfaces of the glass-coated samples sintered at 1350°C for 5 h. (a) alumina + 5% glass, (b) alumina + 15% glass.

4. Conclusions

Pressureless sintering of pure nanocrystalline transition alumina exhibited stable alumina grains with vermicular structure that contained pore networks, and a few micrometer in diameter. Glass-coated samples showed higher phase transformation temperature (i.e., 1400°C in 15 vol% glass) compared to pure alumina (1200°C in pure). The 5 vol% glass-coated sample exhibited much finer microstructure (sub-micron) with respect to pure alumina sample. Excessive amount of the glass (i.e., 15 vol%) enhanced the formation of the intermediate $SrAl_{12}O_{19}$ phase with needle-shape crystals. Segregation of the excess glass to the pellet surfaces was observed during sintering. Consequently, the amount of the glass additive should be controlled below 5 vol% to obtain sintered microstructures appropriate for superplastic deformation.

Acknowledgement

The authors thank the Israel Ministry of Science for supporting this research through the infrastructure grant # 1090-1-98.

References

1. I. LEVIN and D. G. BRANDON, *J. Amer. Ceram. Soc.* **81** (1998) 1995.
2. T. C. CHOU and T. G. NIEH, *ibid.* **74** (1991) 2270.
3. H. HAHN, J. LOGAS and R. S. AVERBACK, *J. Mater. Res.* **5** (1990) 609.
4. R. S. AVERBACK, H. J. HOFLER, H. HAHN and J. C. LOGAS, *NanoStruct. Mater.* **1** (1992) 173.
5. M. J. MAYO and D. C. HAGUE, *ibid.* **3** (1993) 43.
6. P. C. PANDA, J. WANG and R. RAJ, *J. Amer. Ceram. Soc.* **71** (1988) C-507.
7. J. FREIM, J. MCKITTRICK, J. KATZ and K. SICKAFUS, *NanoStruct. Mater.* **4** (1994) 371.
8. R. S. MISHRA, J. SCHNEIDER, J. F. SHACKELFORD and A. K. MUKHERJEE, *ibid.* **5** (1995) 525.
9. M. R. GALLAS, B. HOCKEY, A. PECHENIK and G. J. PIERMARINI, *J. Amer. Ceram. Soc.* **77** (1994) 2107.
10. S.-C. LIAO, Y.-J. CHEN, B. H. KEAR and W. E. MAYO, *NanoStruct. Mater.* **10** (1998) 1063.
11. G. E. GAZZA, J. R. BARFIELD and D. L. PREAS, *Am. Ceram. Soc. Bull.* **48** (1969) 606.
12. Y. ISHOTOBI, M. SHIMADA and M. KOLZUMI, *ibid.* **59** (1980) 1208.
13. R. S. MISHRA, C. E. LESHER and A. K. MUKHERJEE, *J. Amer. Ceram. Soc.* **79** (1996) 2989.
14. C. S. NORDAHL and G. L. MESSING, *ibid.* **79** (1996) 3149.
15. L. A. XUE and I-W. CHEN, *ibid.* **74** (1991) 2011.
16. D. C. BOYD and D. A. THOMPSON, "Kirk-Othmer: Encyclopedia of Chemical Technology," 3rd ed. (John Wiley, N.Y., 1980) Vol. 11, p. 807.
17. M. D. SACKS, N. BOZKURT and G. W. SCHEIFFELE, *J. Amer. Ceram. Soc.* **74** (1991) 2428.
18. J. A. PASK and A. P. TOMSIA, *ibid.* **74** (1991) 2367.
19. J. C. HULLING and G. L. MESSING, *ibid.* **74** (1991) 2374.
20. V. YAROSHENKO and D. S. WILKINSON, *J. Mater. Res.* **15** (2000) 1358.
21. S. C. H. KOH, K. K. AIK and R. MCPERSON, in "Advances in Ceramics," Vol. 24A: Science and Technology of Zirconia III, edited by S. Somiya, N. Yamamoto and H. Hanagida (The AcerS, Westerville, Ohio, 1988) p. 293.
22. W. A. KAYSSER, M. SPRISSLER, C. A. HANDWERKER and J. E. BLENDELL, *J. Amer. Ceram. Soc.* **70** (1987) 339.
23. S. BLONSKI and S. H. GAROFALINI, *ibid.* **80** (1997) 1997.
24. R. BRYDSON, S.-C. CHEN, F. L. RILEY, S. J. MILNE, X. PAN and M. RUHLE, *ibid.* **81** (1998) 369.
25. W. D. KAPLAN, H. MULLEJANS, M. RUHLE, J. RODEL and N. CLAUSSEN, *ibid.* **78** (1995) 2841.
26. B. BLOCH, B. G. RAVI and R. CHAIM, *Mater. Lett.* **42** (2000) 61.
27. D. P. F. DESOUZA and M. F. DESOUZA, *J. Mater. Sci.* **34** (1999) 4023.
28. D. R. CLARKE, *J. Amer. Ceram. Soc.* **70** (1987) 15.

Received 25 June
and accepted 29 November 2001